

Validating diffusion tractography derived connectivity measures of the rat red nucleus and rubrospinal tract using neuroanatomical tracing

Rietberg, T. H.¹, Wielenga, V. H.¹, van Heijningen, C. L.¹, van der Toorn, A.¹, Roeling, T. A. P.², Mackaaij, C.², Verlinde-Schellekens, S. A. M.², Froeling, M.³, Dijkhuizen, R. M.¹.

¹Biomedical MR Imaging and Spectroscopy Group, Center for Image sciences, University Medical Center Utrecht, Utrecht, The Netherlands

²Department of Anatomy, University Medical Center Utrecht, Utrecht, The Netherlands

³Imaging Division, University Medical Center Utrecht, Utrecht, The Netherlands

Layman's Summary

Our bodies and brains are full of water, which is constantly moving around. When water molecules move around freely, they will diffuse randomly and evenly in all directions. In the brain, on the other hand, water molecules tend to move along the fibres of neurons that connect each part of the brain. When an MRI machine is set up in a specific way, it becomes sensitive to the movement of those water molecules. This technique is called diffusion weighted imaging (DWI). The images that are obtained using DWI can then be used to infer the direction of the fibres along which the molecules move. This is called diffusion tractography. Diffusion tractography is very valuable in neuroscientific research. As an example, consider the case of stroke patients. Many people suffer motoric impairments after having a stroke and while some of them recover quite well, others never do. It is suggested that the integrity of a few small neuron fibres such as the rubrospinal tract (RST) might help to explain this difference in outcomes. Diffusion tractography is uniquely qualified as a technique to investigate this in living patients. There is one issue though; tractography algorithms can't be blindly trusted. They need to be validated using other methods. This is where animal models come in handy. Research on animals provides the opportunity to investigate the same sample with neuroanatomical tracing methods, which are considered a golden standard for validating tractography. It entails injecting a solution in the neuron-fibres of interest, which can then be visualised through chemical processes. This study used neuroanatomical tracing to validate diffusion tractography derived connectivity measures of the red nucleus, the point of origin of the RST. The tracing techniques were successful, which provided a database to compare the tractography methods to. This comparison suggests that the algorithms that were used are not quite accurate yet. Although there were some limitations, this finding means that more research should be done before these algorithms can be deemed trustworthy enough for pre-clinical research into recovery after stroke.

Abstract

Diffusion-weighted imaging has become a valuable tool in neuroimaging. However, its accuracy is not guaranteed and a form of validation is often necessary. Animal models prove useful in this regard, because animals can be subjected to histological examination. This study uses histology of the rat brain to validate diffusion tractography of the rubrospinal tract (RST) and the red nucleus (RN) in general. The RST is implicated in motor recovery after stroke. Diffusion tractography analysis of its integrity and plasticity may elucidate its role, potentially forming a target for novel therapies. First, the tractography data on the RST needs to be validated. To this end, neuroanatomical tracer Phaseolus Vulgaris leucoagglutinin (PHA-L) was injected in the RN of three adult female Long Evans rats to trace the RST, after which the brains were subjected to high resolution post-mortem DWI acquisition and immunohistochemical processing. Measures of connectivity strength between the RN and several regions of interest were established in all datasets. These were then used in statistical analysis to determine correspondence between the RST, as well as the RN's connectivity pattern, as described by literature, the histological data and diffusion tractography. The RST could be traced in the histological data, proving that the delivery of PHA-L had been accurate and establishing confidence in the use of these methods for validation. Results show little correspondence between the datasets, suggesting that diffusion tractography analysis does not provide an accurate representation of the RST or the RN's connectivity pattern. This is however a premature conclusion, restricted by several methodological limitations. Follow-up research is therefore needed to confirm or reject these results, before tractography analysis of the RST can be reliably used in a pre-clinical context.

Keywords: red nucleus, rubrospinal tract, tractography, validation, tracing

Contents

Layman’s Summary	2
Abstract	3
Introduction.....	5
Methods	8
Animals and housing	8
Surgical Procedure and Iontophoresis	9
Data acquisition	10
Data processing.....	10
Statistical analysis.....	12
Results.....	13
Discussion	15
Appendix 1.....	20
Appendix 2.....	21
References.....	22

Introduction

The introduction of diffusion-weighted imaging (DWI) in 1985 changed the way scientists viewed the brain both literally and theoretically, as it created the possibility to investigate neural connectivity and plasticity in vivo for the first time (Le Bihan & Breton, 1985). DWI is uniquely sensitive to the displacement of water molecules, which in an unconstrained environment move randomly in an isotropic pattern. In the brain however, this pattern tends to be anisotropic due to the relative ease with which water molecules move parallel to white matter fibres as opposed to perpendicularly (Assaf et al., 2004). It is this fundamental quality that lies at the heart of a technique called tractography.

Tractography is the reconstruction of white matter pathways based on the diffusion patterns of water molecules in the brain (Conturo et al., 1999). It has become an essential tool in neuroimaging and is being used in a wide range of contexts, from the planning of neurosurgery (Clark et al., 2003) to broader studies of connectomics such as the Human Connectome Project (NIH, n.d.). In its simplest form, tractography relies on the diffusion tensor of each voxel, which is essentially a 3-dimensional covariance matrix of water molecule displacement (Tournier, 2019) and can be represented as an ellipsoid, the circumference of which reflects relative anisotropy. The orientation of the primary axis along which diffusion occurs is represented by the principal eigenvector of the matrix (Tournier, 2019), which can simply be traced from voxel to voxel to infer white matter trajectory. It is this simplicity, however, that lies at the heart of some critical issues.

Since MRI voxels are typically on a scale of hundreds of microns up to millimetres, each voxel may contain thousands of neurons. Their configurations are far from straightforward, thus assigning a single diffusion direction to each voxel will inevitably misrepresent reality in many cases. Using the diffusion tensor to infer white matter

trajectories is especially problematic in regions with many crossing, kissing or fanning fibres (Schilling et al., 2019b; Tournier, 2019).

For this reason, many alternatives for diffusion tensor imaging (DTI) have been developed. Examples include Q-ball imaging (Tuch, 2004), which relies on high angular resolution diffusion imaging (HARDI; Descoteaux, 1999) to estimate the diffusion orientation density function (dODF) (Wedeen et al., 2005). This can then be transformed to the fibre orientation density function (fODF), which can be used to perform tractography analysis. Other methods use a predictive model of the signal that would be expected for a given fibre orientation to directly estimate the fODF. These include multi-tensor fitting (Tuch et al., 2002) and constrained spherical deconvolution (CSD; Tournier et al., 2004). Especially the latter is capable of tracking intricate networks of fibres more accurately.

Further errors can however occur at any other stage of the process. It is well established that DWI is noisy and prone to artifacts, for example due to eddy currents. Due to the high sensitivity to water displacement on a micron scale, DWI is also greatly influenced by subject motion during acquisition (Pierpaoli, 2010; Le Bihan et al., 2006). These artifacts can lead to bias, uncertainty and distortion, which contribute to inaccuracies in tractography. Finally, the process of tracking fibres from voxel to voxel is prone to error due to the length and shape of streamlines and choices of tracking parameters such as step size, curvature thresholds and seeding or stopping criteria (Thomas et al., 2014).

From all these considerations it becomes clear that even when measures are taken to minimize the mentioned sources of error, it remains essential to validate tractography with other sources of anatomical knowledge. These include existing literature or atlases concerning the expected connectivity pattern of a specific region. Furthermore, histological examination, preferably of the same sample, can be used to establish accuracy measures (e.g. Dauguet et al., 2007; Gao et al., 2013; Schilling et al., 2019a).

This is where animal models prove valuable. Since histological examination can exclusively be done post-mortem, it's not a feasible validation technique in clinical studies on humans. In contrast, in pre-clinical animal models the subjects can be sacrificed and their tissue immediately fixated, after which post-mortem DWI acquisition and histological examination can ensue. This allows for longer acquisition times which, combined with ultra-high field scanners, results in DWI-data with an exceptionally high resolution. Furthermore, this ensures that the tissue is minimally altered before being examined histologically. With these advantages in mind the present study used such a set-up, in combination with pre-existing knowledge collected in NeuroVIISAS (Schmitt & Eipert, 2012) to validate DWI-based measures of connectivity of the red nucleus (RN), including the rubrospinal tract (RST), in the rat brain.

The RST is part of a group of small descending tracts involved in motor control (Felten et al., 2016). Relative to the corticospinal tract (CST), its function is less clearly understood. For instance, when damage occurs to the motor system as a result of ischaemic stroke, the CST alone cannot fully explain why some patients recover and others remain motorically impaired. Thus, these smaller descending tracts presumably play an important role which isn't yet elucidated. Investigations into the connectivity and plasticity of the RN and RST may shed light on this issue and perhaps guide development of novel therapies. Pre-clinical tractography analysis provides the unique tools to perform these investigations, but for the reasons described above a form of validation is essential before the data can be properly analysed.

The present study was set up to gain insight into the anatomy of the RST and to validate the diffusion tractography derived reconstruction of the RST and connectivity of the RN in general. To this end, neuroanatomical tracer Phaseolus Vulgaris leucoagglutinin (PHA-L; Gerfen & Sawchenko, 1984) was injected in the RN of 3 adult female Long-Evans rats.

PHA-L is taken up by neuronal cell-bodies, where it is incorporated in the cytoplasm and actively transported towards the axon-terminals. PHA-L can be visualized using immunohistochemical processes, thereby elucidating connections between the location of injection and the rest of the brain.

Neuroanatomical tracing methods of this kind are considered the golden standard of structural connectivity analysis. By establishing connectivity measures between the RN and other regions of interest (ROIs) using neuroanatomical tracing as well as diffusion tractography in the same sample, the connectivity pattern as described by the latter method can be validated by comparison to this pattern as described by the first.

The connectivity pattern in histological data is hypothesized to correlate positively with the DWI data, with the connectivity patterns according to CSD algorithms showing a stronger correlation than those according to DTI. Besides, based on literature (e.g. Felten et al., 2016), the RST is expected to be more prominent contralateral to the injection. The results will form a foundation for further investigations into the RN and RST in particular, as well as contributing to the general literature on tractography validation.

Methods

Animals and housing

For final data acquisition, three healthy adult (18 weeks) female Long-Evans rats (Charles River, Italy) were used. The animals were fed standard chow ad libitum and housed in standard grouped cages. All procedures were approved by the Animal Experiments Committee of the University Medical Centre Utrecht and Utrecht University and were performed according to the guidelines of the European Communities council Directive and Dutch law ('Wet op de Dierproeven', 2014).

Surgical Procedure and Iontophoresis

Rats were fully anaesthetized using isoflurane (5% for induction, 2.5% for maintenance in air/O² (4:1)) and placed in a stereotactic frame. 100µl Lidocaine was applied subcutaneously on the head and part of the skull was cleared of all tissue and periosteum. A small hole was then drilled to allow for a glass capillary micropipette (1mm external Ø, 0.58mm internal Ø, Hilgenberg GMBH) to be inserted intracerebrally. The pipettes were pulled on a sutter instrument prior to the surgery to create a very narrow tip, which minimizes unintended damage to the brain tissue.

Prior to insertion, a 2.5% solution of PHA-L (Vector Labs) was loaded into the pipette by placing the tip in a 10µl aliquot. A platinum wire was inserted into the solution in the pipette and connected to the negative terminal of an iontophoresis device, whereas the positive terminal was connected to the rat's hind paw. After external cleaning of the pipette to reduce dragging PHA-L along the needle tract, the pipette was inserted at coordinates -5.6mm (AP), 1.5mm (ML) and -7.6mm (DV, from skull) relative to Bregma to target the RN.

For iontophoretic delivery of PHA-L, the iontophoresis device was set to negative polarity so that current would flow from the negative to the positive terminal. The current alternated between 0 and 5 µAmp with intervals of 6 seconds for a total time of 10 minutes. After these 10 minutes the device was switched off and the rats remained stationary with the pipette still in place for another 20 minutes. After the pipette was removed, the rats were allowed to recover and carprofen (5mg/kg bodyweight) was administered subcutaneously for analgesia.

After 7 days the rats were euthanised by an overdose of isoflurane, followed by transcardial perfusion fixation. During perfusion, 100ml 0.9% NaCL with 1ml/L heparine was used to flush the blood from all vessels. Subsequently, 250ml 4% paraformaldehyde (PFA) was used to fixate the tissue. The skulls were then prepared for post mortem MRI scanning.

All tissue was removed and the skulls were kept in PFA for a week, after which they were placed in phosphate buffered saline (PBS) with azide. After five more days, air was removed from the skulls and brains using a vacuum desiccator. Just prior to MRI, the skulls were transferred to Galden.

Data acquisition

DWI

Post-mortem DWI was performed on a 9.4T horizontal bore preclinical Varian MR system (Palo Alto, CA, USA), equipped with a gradient (60mm internal Ø) with a maximum strength of 1000 mT/m. A vertically oriented RF coil (26mm internal Ø) was used. Diffusion-weighted MRI was acquired using a SE-EPI sequence at 150µm isotropic resolution in 110 diffusion-weighted directions, increasingly divided over 5 b-values: 0, 2500, 5000, 7500, 10000. During acquisition a constant temperature of ~17.5°C was maintained to eliminate temperature-related changes in diffusion.

Histology

When the MRI acquisition was completed, the brains were removed from the skull and kept in a 30% sucrose solution for 5 days in preparation of histological processing. The brains were then cut frozen on a microtome in the coronal plane at 40µm intervals and coupes were collected free-floating in 8 wells filled with PBS. Coupes from one of these wells were used for further processing, so that the interval between processed coupes was 320µm.

These coupes were processed to allow diaminobenzidine (DAB)-staining of PHA-L, and then counterstained with Haematoxylin. For the full staining protocol used, see Appendix 1.

Data processing

NeuroVIISAS

The list of ROIs obtained from NeuroVIISAS (Schmitt & Eipert, 2012) was filtered so that only ROIs that were also found in the histological datasets remained. Furthermore, the ordinal

system by which connectivity strength is presented on the NeuroVIISAS website was used to exclusively select ROIs that either had a score of 0 or ≥ 2 . See Appendix 2 for the filtered list of ROIs.

DWI

First, the acquired volumes were denoised and motion corrected. Severe distortions were present for one of the rats, which could not be corrected for. Data from this rat has therefore not been included in further analysis. For the two remaining datasets the MRTrix 3.0 software (Tournier et al, 2019) was used to perform deterministic and probabilistic CSD, as well as deterministic and probabilistic DTI and structural connectivity analysis. ROIs (Appendix 2) were drawn according to Paxinos and Watson's stereotactic rat brain atlas (Paxinos & Watson, 2005) and registered to a mean diffusion weighted volume for each rat.

These ROIs were compiled into parcellation images which were used according to the 'Structural connectome construction' guide on the MRTrix website to extract a matrix containing the number of streamlines between the Red Nucleus and each individual ROI specifically. These connectivity matrices were then normalized using fractional scaling as described in Donahue (2016). The number of streamlines between RN and each ROI was divided by the sum of all streamlines connected to both regions respectively, excluding self-connections. The resulting weights represent the fraction of streamlines (Delettre et al, 2019), which was used as a measure of connectivity strength in further analysis.

Histology

The stained coupes were digitised using a Leica digital microscope at 10x magnification. In these images, DAB was split from Haematoxylin using the *Colour Deconvolution 2* plugin in ImageJ. The split DAB images were then converted to 8 bit and inverted, which allowed for thresholding to filter pixels containing actual DAB from background noise. See *Figure 1* for an example of this process. Target ROIs (Appendix 2) were drawn according to Paxinos and

Watson's stereotactic rat brain atlas (Paxinos & Watson, 2005). An important sidenote here is that due to the cutting and staining procedure that was used, it was impossible to distinguish left from right in the digitalized coupes. Assigning sides as either ipsi- or contralateral relative to the injection site was therefore done based on the assumption that the contralateral side would have more tracer present. Finally, ImageJ's particle analysis function was used to calculate the percentage of pixels within the ROIs that contained DAB. This was used as a measure of connectivity strength in further analysis.

Statistical analysis

Before analysis, all except the ordinal NeuroVIISAS (Schmitt & Eipert, 2012) values were log₁₀-transformed to accommodate for a right-skewed distribution. All data approximated normal distribution after transformation. The log₁₀-transformed data was used in Pearson's correlation analysis to establish correspondence in ROI-based connectivity of the RN between histological data and MRI tractography.

Before conducting ANOVA analysis to determine correspondence between connectivity strength according to neuroVIISAS (Schmitt & Eipert, 2012) and histological and MRI data, it was determined that several assumptions were violated in the neuroVIISAS (Schmitt & Eipert, 2012) dataset. These included the assumption of normality, which could not be solved

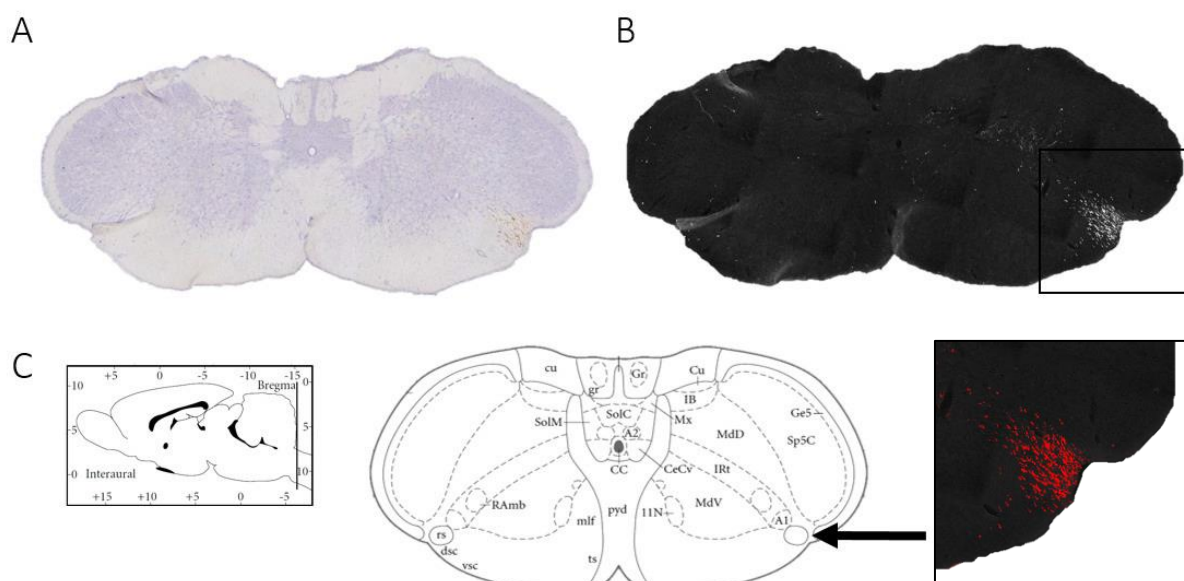


Figure 1. Example of processing in ImageJ

by transformation due to the nature of the underlying reality upon which the ordinal categories were based, and heteroscedasticity. Furthermore, two of the categories contained only one datapoint and there was no equal number of datapoints across categories. Therefore, no analysis could properly be conducted on this data.

Results

A similar connectivity pattern was present across the four different tractography algorithms, as can be seen in Table 1. The mesencephalic reticular formation and pontine reticular nucleus were the most prominent connections in all four algorithms, with the cuneate nucleus also being strongly connected to the RN according to both DTI algorithms.

Connection strength between RN and the ROI representing the contralateral RST was below average, however not significantly, across all algorithms and both rats. Z-score for this ROI in rat #1 in deterministic CSD was -0.19 ($p = .42$) and in probabilistic CSD -0.06 ($p = .48$). In deterministic DTI it was -0.15 ($p = .44$) and in probabilistic DTI -0.08 ($p = .47$). For rat #2, in the same order, z-scores were -0.60 ($p = .27$), -0.43 ($p = .34$), -1.47 ($p = .07$) and -1.13 ($p = .13$).

The histological data shows a different pattern altogether, as can be seen in columns 5 and 10 of Table 1. The olivary nucleus shows a strong connection in rat #1 but not in rat #2. No other areas have a connectivity strength which differs significantly from the others, except the contralateral RST in rat #2. In the histological data for this rat, the z-score for the RST was 2.07 ($p = .03$). For rat #1 this was 1.52 ($p = .06$).

These differing patterns of connectivity within the DWI data as opposed to histological data are reflected in the correlation analysis, the results of which can be found in *Figure 2* and Table 2.

Table 1. Connection strengths in both rats between the Left Red Nucleus and all other ROIs. Shown are the results for deterministic and probabilistic CSD and DTI, measured in the fraction of streamlines and for histology, measured in the percentage of the total area of the ROI that was covered by DAB-staining. Higher scores represented by darker green.

Structure	Ipsi-or Contralateral	Rat #1					Rat #2				
		Fraction of Streamlines		% of Area			Fraction of Streamlines		% of Area		
		Det. CSD	Prob. CSD	Det. DTI	Prob. DTI	Histo	Det. CSD	Prob. CSD	Det. DTI	Prob. DTI	Histo
Abducens System	Ipsi	0,0169	0,0124	0,0244	0,0403	0,3600	0,0119	0,0142	0,0138	0,0207	0,6400
	Contra	0,0029	0,0076	0,0091	0,0202	0,0200	0,0073	0,0108	0,0135	0,0188	1,2900
Facial Nucleus	Ipsi	0,0092	0,0167	0,0542	0,0267	0,5300	0,0099	0,0170	0,0487	0,0302	0,5500
	Contra	0,0043	0,0073	0,0247	0,0106	0,6900	0,0070	0,0054	0,0302	0,0239	2,1700
Cuneate Nucleus	Ipsi	0,0153	0,0222	0,1191	0,0988	0,2200	0,0182	0,0248	0,1212	0,1048	0,1200
	Contra	0,0100	0,0115	0,0572	0,0448	0,1400	0,0097	0,0141	0,0716	0,0635	0,7800
Lateral Reticular Nucleus	Ipsi	0,0111	0,0173	0,0305	0,0354	0,0600	0,0129	0,0175	0,0367	0,0352	0,2400
	Contra	0,0037	0,0075	0,0057	0,0064	0,3000	0,0021	0,0052	0,0185	0,0108	0,2100
Mesencephalic Reticular Formation, dorsal part	Ipsi	0,1103	0,0952	0,0581	0,0893	0,2200	0,1163	0,1104	0,0716	0,0864	0,0700
	Contra	0,0697	0,0734	0,0456	0,0502	0,1500	0,0636	0,0717	0,0676	0,0741	0,2000
Mesencephalic Reticular Formation, ventral part	Ipsi	0,0125	0,0052	0,0015	0,0007	0,7100	0,0191	0,0145	0,0033	0,0031	0,6300
	Contra	0,0130	0,0073	0,0020	0,0007	0,3300	0,0116	0,0079	0,0005	0,0010	1,0800
Medullary Reticular Nucleus, dorsal part	Ipsi	0,0007	0,0021	0,0046	0,0047	0,1800	0,0018	0,0027	0,0138	0,0123	0,4700
	Contra	0,0005	0,0011	0,0054	0,0064	0,1600	0,0009	0,0015	0,0104	0,0087	2,5300
Olivary Nucleus	Ipsi	0,0125	0,0241	0,0043	0,0122	5,9200	0,0147	0,0234	0,0051	0,0157	1,4000
	Contra	0,0038	0,0144	0,0081	0,0111	2,2200	0,0039	0,0069	0,0076	0,0053	0,5900
Pontine Reticular Nucleus	Ipsi	0,0985	0,0805	0,0880	0,1098	1,1300	0,1185	0,0985	0,0535	0,0743	1,1800
	Contra	0,0378	0,0355	0,0579	0,0330	0,9100	0,0523	0,0408	0,0361	0,0285	0,8000
Raphe Magnus Nucleus	Central	0,0071	0,0115	0,0088	0,0059	2,4800	0,0022	0,0086	0,0067	0,0079	1,4300
Raphe Pallidus Nucleus	Central	0,0013	0,0045	0,0026	0,0041	1,5900	0,0026	0,0056	0,0011	0,0032	0,3400
Rubrospinal Tract	Ipsi	0,0112	0,0178	0,0366	0,0543	0,5300	0,0159	0,0165	0,0197	0,0293	1,2700
	Contra	0,0067	0,0121	0,0125	0,0139	3,7400	0,0046	0,0085	0,0017	0,0042	5,9200

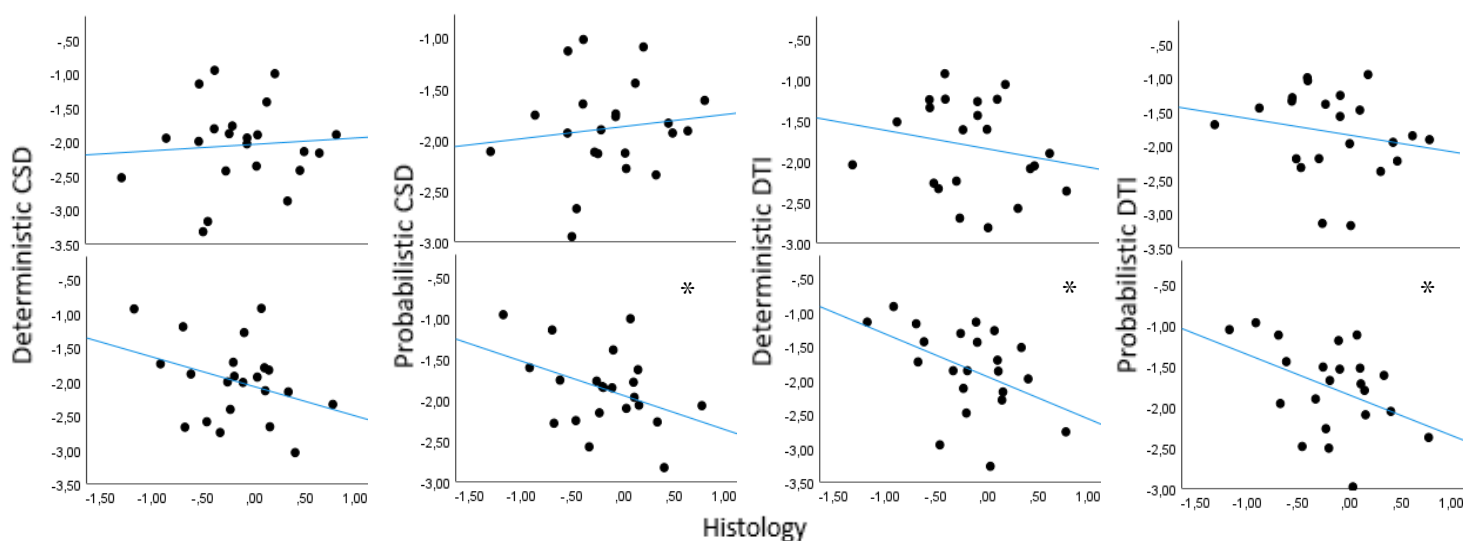


Figure 2. Visualisation of the correlations found in Table 2 for rat #1 on top and rat #2 on the bottom.

*. Correlation is significant at the 0.05 level (1-tailed).

Table 2. Correlations between the connectivity strengths as determined within deterministic and probabilistic CSD and DTI and histology for both rats.

		Rat #1					Rat #2				
		Det. CSD	Prob. CSD	Det. DTI	Prob. DTI	Histo	Det. CSD	Prob. CSD	Det. DTI	Prob. DTI	Histo
Deterministic CSD	r	--					--				
Probabilistic CSD	r	,926**	--				,954**	--			
	p	0,000					0,000				
Deterministic DTI	r	,596**	,688**	--			,459*	,503**	--		
	p	0,002	0,000				0,016	0,009			
Probabilistic DTI	r	,523**	,691**	,923**	--		,572**	,633**	,952**	--	
	p	0,006	0,000	0,000			0,003	0,001	0,000		
Histology	r	0,077	0,126	-0,201	-0,199	--	-0,346	-,409*	-,456*	-,423*	--
	p	0,367	0,288	0,185	0,187		0,057	0,029	0,016	0,025	

** . Correlation is significant at the 0.01 level (1-tailed).

* . Correlation is significant at the 0.05 level (1-tailed).

Discussion

Diffusion tractography is a valuable tool in neuroimaging, used in contexts ranging from neurosurgery (Clark et al., 2003) to broader studies of connectomics (NIH, n.d.). Its unique sensitivity to water displacement creates the opportunity to track the direction of diffusion from voxel to voxel, thereby tracing fibres of axons (Tournier, 2019). This principle allows for *in vivo* examination of structural connectivity and plasticity. However, since a single voxel typically contains thousands of neurons, assigning a single diffusion direction per voxel is inherently problematic (Schilling et al., 2019b; Tournier, 2019). Algorithms such as CSD are better equipped to deal with issues of crossing, kissing and fanning fibres, yet errors can still occur at any step of the process (Pierpaoli, 2010; Le Bihan et al., 2006). Therefore, a form of validation is necessary before diffusion tractography data can be reliably analysed. Here, animal models prove valuable because the animals can be subjected to histological examination.

Combined with pre-existing knowledge found on the NeuroVIISAS website (Schmitt & Eipert, 2009), this study used neuroanatomical tracing to validate diffusion tractography of the RN in the rat brain. The RN is the point of origin for the RST, which is implicated in

potential motor recovery after stroke. Investigations into its plasticity using diffusion tractography in rats may elucidate its role in the recovery process of stroke patients, potentially forming a target for novel therapies. Before drawing conclusions from tractography data on the RST, the current study was set up to confirm its validity. The aim of this study was to gain insight into the anatomy of the RST and to validate the diffusion tractography derived reconstruction of the RST and general connectivity pattern of the RN using neuroanatomical tracing.

Based on literature (e.g. Felten et al., 2016), it was expected that the RST would be more prominently represented contralaterally to the injection site. Moreover, connectivity strength as determined from histological examination was expected to positively correlate to connectivity strengths from tractography analyses.

First of all, the histological data strongly indicates a tract corresponding to the RST as it is described in literature (for an example, see *Figure 1*). This result shows that the tracer was successfully delivered to the RN and that the RN does indeed form the point of origin for the RST. However, the lack of discrimination between left and right renders this data incapable of confirming that the RST crosses the midline and continues its path contralaterally. Such a conclusion would be biased due to previously mentioned method of assigning sides as either ipsi-or contralateral. Nevertheless, this result provides confidence in the methods used and is a key element in further analysis.

In contrast to the histological data, the diffusion tractography data doesn't show a clearly distinguishable RST. Assuming the tract's contra-laterality, this lack of connectivity between RN and RST might be due to certain choices in parameter settings such as the curvature threshold, since most algorithms had difficulties crossing the midline at all. Further research using methodological improvements allowing for discrimination of left and right in

the histological data is needed to confirm the RST's contra-laterality and determine whether these results reflect inaccuracies in the tractography algorithms, or true anatomy.

The latter hypothesis stated that connectivity strength in histological data would be positively correlated to connectivity strength in diffusion tractography data. This was not found in this study. No correlation was found in one of the rats, while a negative correlation was found in three out of four algorithms for rat #2. In other words, the stronger an ROI was connected to the RN in histological data, the weaker this connection was in the DWI data. These findings suggests that the diffusion tractography algorithms do not provide an accurate description of the structural connectivity of the RN. This is however a premature conclusion, which is clouded by a very limited sample size as well as a few other methodological limitations.

For instance, in the absence of a more robust technique, ROIs were drawn and adjusted manually in both the DWI and histological data. This proved to be challenging. Especially in the histological data this method is susceptible to high intra- and inter-researcher variability, which makes the experiment difficult to repeat reliably. To improve on this issue, corresponding images from Paxinos and Watson's (2005) atlas were overlaid on the histological scans. However, due to deformations an entirely accurate overlay could not be achieved for some coupes. As a result, the ROIs that were used in analysis may not have been an accurate representation of these regions in reality.

For DWI data, registration procedures were used to transfer adapted ROIs from the atlas directly to subject MRI space, improving the repeatability and standardization. The registration process did however impose certain subtle deformations on the ROIs, which required slight manual adjustment. Nonetheless, creating ROIs through registration is more accurate and reliable than a completely manual process. A similar registration procedure would therefore benefit the ROIs in the histological data as well.

A final and important consideration is whether the neuroanatomical tracing data can indeed be considered as ground truth for diffusion tractography validation. Several differences between the methods make for a complicated comparison. For instance, the starting point of a tract in tractography doesn't necessarily represent the starting point of neurons. Similarly, the algorithm doesn't stop at the synaptic terminal. PHA-L on the other hand is transported only within a single neuron, and only anterogradely. In contrast, the amount of streamlines measured between the RN and any ROI contained streamlines in both directions. What is being measured in these methods is therefore not entirely the same, putting the tracing data's role as ground truth in question.

Together, these limitations impose restrictions on any conclusions that can be drawn from this study. Nevertheless, the preliminary results seem to point towards an incongruity between neuroanatomical tracing and diffusion tractography from the red nucleus. Follow-up research is needed in which aforementioned limitations are overcome to determine whether these results reflect reality. In that case the algorithms need to be subjected to rigorous optimisation and validation procedures before a reliable conclusion can be drawn from their results.

To overcome the limitations, several improvements can be made. For instance, by making use of a tracer that is transported trans-synaptically and is taken up by fibres of passage, a comparison between neuroanatomical tracing data and tractography is more justified than it is when using PHA-L. Furthermore, a researcher performing paraffine cutting will always be able to distinguish left from right. This provides the means to confirm the finding that the RST is indeed most prominent on the contralateral side. Moreover, using paraffine cutting and a mounted staining procedure instead of a free-floating procedure could minimize deformations during the process, thereby making more accurate ROIs possible.

To avoid the inherent issues of drawing ROIs completely, one may consider a processing pipeline in which the histological scans are compiled into a three dimensional image, which can be registered to the MRI data. The tracer's presence in the brain can then be delineated and binarized into a mask. Measures of overlap between this mask and the tractogram can then be calculated, which would allow for a more specific validation of the RST. See Dauguet et al. (2007), Gao et al. (2013) and Schilling et al. (2019a) for examples of such a pipeline.

In conclusion, neuroanatomical tracing methods used in this study confirmed the presence of the RST as it is described in literature. This result establishes confidence in the use of these methods to validate diffusion tractography data on the RST and the RN in general. Preliminary results on that matter show incongruencies between the tracing data and DWI data, which suggests that the diffusion tractography algorithms do not provide an accurate description of the connectivity pattern of the RN or the RST. This conclusion is however clouded by several methodological limitations. Since the RST is implied in a clinical context and may eventually form a target for novel therapies in stroke patients, the diffusion tractography used in its investigation needs to perform accurately and reliably. Follow-up research is therefore needed to confirm or reject the results of this study, before tractography analysis can be used in further pre-clinical investigations of the RST.

Appendix 1 – Free floating DAB-staining protocol for PHA-L

Day 1

Rinse (PBS)	3 x 10'
3% H ₂ O ₂ in methanol (1ml 30% H ₂ O ₂ in 9ml methanol)	20'
Rinse (PBS)	3 x 10'
Block: PBST (PBS + Triton 0.1%) + Normal Goat Serum (NGS) (20%)	30' RT
PBST + Rabbit anti-Pha-L (1 : 1000)	O/N 4°C

Day 2

Rinse (PBS)	3 x 10'
2nd Antibody: PBST + Goat anti-Rabbit 1:400	60' RT
Rinse (PBS)	3 x 10'
ABC: 10µL A & 10µL B in 1 ml PBS (covered with aluminium foil)	60' RT
Rinse (PBS)	2 x 10'
Tris-Hcl	5'
DAB (1mg DAB per 2ml 0.05M Tris-HCl, right before use add H ₂ O ₂ at 3µL:10ml)	1 - 5'

Transfer onto glass slides

Counterstaining

Demiwater	1-5min
Haematoxylin (diluted; He:Demiwater 15:11)	7 dips
Rinse (tapwater)	30s
Demiwater	30s

Dehydration

Ethanol: 70% > 96% > 100% > 100% > xyleen > xyleen	10s each
--	----------

Mount coverslip

Appendix 2 – filtered list of target ROIs taken from NeuroVIISAS

(Schmitt & Eipert, 2012)

<https://neuroviisas.med.uni-rostock.de/connectome/index.php>

Structure	Ipsi- or contralateral	Connectivity strength (max = 4)
Abducens System	Ipsilateral	n/a
	Contralateral	3
Facial Nucleus	Ipsilateral	2
	Contralateral	3
Cuneate Nucleus	Ipsilateral	2.5
	Contralateral	n/a
Lateral Reticular Nucleus	Ipsilateral	4
	Contralateral	n/a
Mesencephalic Reticular Formation, dorsal part	Ipsilateral	3
	Contralateral	n/a
Mesencephalic Reticular Formation, ventral part	Ipsilateral	3
	Contralateral	n/a
Medullary Reticular Nucleus, dorsal part	Ipsilateral	n/a
	Contralateral	4
Olivary Nucleus	Ipsilateral	0
	Contralateral	n/a
Pontine Reticular Nucleus	Ipsilateral	3
	Contralateral	0
Raphe Magnus Nucleus	Central	0
Raphe Pallidus Nucleus	Central	4

References

- Assaf, Y., Freidlin, R. Z., Rohde, G. K., & Basser, P. J. (2004). New modeling and experimental framework to characterize hindered and restricted water diffusion in brain white matter. *Magnetic Resonance in Medicine*, *52*(5), 965–978. <https://doi.org/10.1002/mrm.20274>
- Clark, C. A., Barrick, T. R., Murphy, M. M., & Bell, B. A. (2003). White matter fiber tracking in patients with space-occupying lesions of the brain: A new technique for neurosurgical planning? *NeuroImage*, *20*(3), 1601–1608. <https://doi.org/10.1016/j.neuroimage.2003.07.022>
- Conturo, T. E., Lori, N. F., Cull, T. S., Akbudak, E., Snyder, A. Z., Shimony, J. S., McKinstry, R. C., Burton, H., & Raichle, M. E. (1999). Tracking neuronal fiber pathways in the living human brain. *Proceedings of the National Academy of Sciences*, *96*(18), 10422–10427. <https://doi.org/10.1073/pnas.96.18.10422>
- Dauguet, J., Peled, S., Berezovskii, V., Delzescaux, T., Warfield, S. K., Born, R., & Westin, C.-F. (2007). Comparison of fiber tracts derived from in-vivo dti tractography with 3D histological neural tract tracer reconstruction on a macaque brain. *NeuroImage*, *37*(2), 530–538. <https://doi.org/10.1016/j.neuroimage.2007.04.067>
- Delettre, C., Messé, A., Dell, L. A., Foubet, O., Heuer, K., Larrat, B., Meriaux, S., Mangin, J. F., Reillo, I., de Juan Romero, C., Borrell, V., Toro, R., & Hilgetag, C. C. (2019). Comparison between diffusion MRI tractography and histological tract-tracing of cortico-cortical structural connectivity in the ferret brain. *Network neuroscience (Cambridge, Mass.)*, *3*(4), 1038–1050. https://doi.org/10.1162/netn_a_00098
- Descoteaux, M. (1999). High angular resolution diffusion imaging (Hardi). *Wiley Encyclopedia of Electrical and Electronics Engineering*, 1–25. <https://doi.org/10.1002/047134608x.w8258>
- Donahue, C. J., Sotiropoulos, S. N., Jbabdi, S., Hernandez-Fernandez, M., Behrens, T. E., Dyrby, T. B., Coalson, T., Kennedy, H., Knoblauch, K., Van Essen, D. C., & Glasser, M. F. (2016). Using Diffusion Tractography to Predict Cortical Connection Strength and Distance: A Quantitative Comparison with Tracers in the Monkey. *The Journal of neuroscience : the official journal of the Society for Neuroscience*, *36*(25), 6758–6770. <https://doi.org/10.1523/JNEUROSCI.0493-16.2016>

- Felten, D. L., O'Banion, M. K., & Maida, M. S. (2016). Motor systems. *Netter's Atlas of Neuroscience*, 391–420. <https://doi.org/10.1016/b978-0-323-26511-9.00015-1>
- Gao, Y., Choe, A. S., Stepniewska, I., Li, X., Avison, M. J., & Anderson, A. W. (2013). Validation of DTI Tractography-based measures of primary motor area connectivity in the squirrel monkey brain. *PLoS ONE*, 8(10). <https://doi.org/10.1371/journal.pone.0075065>
- Gerfen, C. R., & Sawchenko, P. E. (1984). An anterograde neuroanatomical tracing method that shows the detailed morphology of neurons, their axons and terminals: Immunohistochemical localization of an axonally transported plant lectin, Phaseolus vulgaris leucoagglutinin (Pha-L). *Brain Research*, 290(2), 219–238. [https://doi.org/10.1016/0006-8993\(84\)90940-5](https://doi.org/10.1016/0006-8993(84)90940-5)
- Hebb, D. O. (1949). *The organization of behaviour: A neuropsychological theory*. New York: Wiley and Sons.
- Le Bihan, D., & Breton, E. (Nov 1985). In vivo magnetic resonance imaging of diffusion. *Comptes Rendus des Seances de l'Academie des Sciences Serie 2*, 301(15), 1109-1112.
- Le Bihan, D., Poupon, C., Amadon, A., & Lethimonnier, F. (2006). Artifacts and pitfalls in Diffusion MRI. *Journal of Magnetic Resonance Imaging*, 24(3), 478–488. <https://doi.org/10.1002/jmri.20683>
- National Institutes of Health. (n.d.). *HCP - Overview of the Human Connectome Project*. Human Connectome Project. Retrieved October 20, 2021, from <https://www.humanconnectome.org/study/hcp-young-adult/overview>.
- Paxinos, G., & Watson, C. (2005). *Paxinos & Watson, The Rat Brain in stereotaxic coordinates* (5th ed.). Elsevier Academic Press.
- Pierpaoli, C. (2010). Artifacts in diffusion MRI. *Diffusion MRI*, 303–318. <https://doi.org/10.1093/med/9780195369779.003.0018>
- Schilling, K. G., Gao, Y., Stepniewska, I., Janve, V., Landman, B. A., & Anderson, A. W. (2019a). Anatomical accuracy of standard-practice tractography algorithms in the motor system - a histological validation in the squirrel monkey brain. *Magnetic Resonance Imaging*, 55, 7–25. <https://doi.org/10.1016/j.mri.2018.09.004>
- Schilling, K. G., Nath, V., Hansen, C., Parvathaneni, P., Blaber, J., Gao, Y., Neher, P., Aydogan, D. B., Shi, Y., Ocampo-Pineda, M., Schiavi, S., Daducci, A., Girard, G., Barakovic, M., Rafael-Patino, J., Romascano, D., Rensonnet, G., Pizzolato, M., Bates, A., ... Landman, B. A. (2019b). Limits to anatomical accuracy of diffusion

- tractography using modern approaches. *NeuroImage*, 185, 1–11.
<https://doi.org/10.1016/j.neuroimage.2018.10.029>
- Schmitt, O., & Eipert, P. (2012). neuroVIISAS: Approaching Multiscale Simulation of the Rat Connectome. *Neuroinformatics*, 10(3), 243-67. doi: 10.1007/s12021-012-9141-6
- Thomas, C., Ye, F. Q., Irfanoglu, M. O., Modi, P., Saleem, K. S., Leopold, D. A., & Pierpaoli, C. (2014). Anatomical accuracy of brain connections derived from diffusion MRI tractography is inherently limited. *Proceedings of the National Academy of Sciences*, 111(46), 16574–16579. <https://doi.org/10.1073/pnas.1405672111>
- Tournier, J. D. (2019). Diffusion MRI in the brain – theory and concepts. *Progress in Nuclear Magnetic Resonance Spectroscopy*, 112-113, 1–16.
<https://doi.org/10.1016/j.pnmrs.2019.03.001>
- Tournier, J.-D., Calamante, F., Gadian, D. G., & Connelly, A. (2004). Direct estimation of the fiber orientation density function from diffusion-weighted MRI data using spherical deconvolution. *NeuroImage*, 23(3), 1176–1185.
<https://doi.org/10.1016/j.neuroimage.2004.07.037>
- Tournier, J.-D., Smith, R. E., Raffelt, D., Tabbara, R., Dhollander, T., Pietsch, M., Christiaens., D, Jeurissen, B., Yeh, C.-H., & Connelly, A. (2019). *MRtrix3*: A fast, flexible and open software framework for medical image processing and visualisation. *NeuroImage*, 202, 116–37.
- Tuch, D. S. (2004). Q-ball imaging. *Magnetic Resonance in Medicine*, 52(6), 1358–1372.
<https://doi.org/10.1002/mrm.20279>
- Tuch, D. S., Reese, T. G., Wiegell, M. R., Makris, N., Belliveau, J. W., & Wedeen, V. J. (2002). High angular resolution diffusion imaging reveals intravoxel white matter fiber heterogeneity. *Magnetic Resonance in Medicine*, 48(4), 577–582.
<https://doi.org/10.1002/mrm.10268>
- Wedeen, V. J., Hagmann, P., Tseng, W.-Y. I., Reese, T. G., & Weisskoff, R. M. (2005). Mapping complex tissue architecture with diffusion spectrum magnetic resonance imaging. *Magnetic Resonance in Medicine*, 54(6), 1377–1386.
<https://doi.org/10.1002/mrm.20642>